Rover model ejection and landing performance comparison analysis

Kaylee La Spisa, Clare Reilly

1. Introduction

1.1 Models Compared and Stress Case Studies

Finite element simulations are useful in examining how the representation of a real life model could react when certain boundary conditions are applied during testing. Without the need to already have a physical testing situation to gain information, many different scenarios can be performed by a computer. As an example of real application, a team that is having difficulty choosing between two model designs may use a finite element analysis to decide which model will move forward into the production and testing phases without having to w savvy svwcw a prototype and run tests for each of them first. This report hopes to make such a conclusion for a currently ongoing studssxxsttrdhvent project by comparing the two proposed models of rovers and simulating the launching and landing forces each would experience. The outcome of the simulations will help prove one model more suited for the upcoming launch, and so will allow it to move on to production.

1.2 Relevance & Simulations

A simulated analysis will save the team both the time and cost of creating two separate models. This report will examine six cases of stress tests that the rovers will face in a real situation and need to pass to be successful. There will be three simulations for each model, and all will be represented as closely to an ideal testing situation as possible. These six cases are listed below:

- Simulation #1, Ejection from Rocket Case #1: non-finned rover is simulated as ejecting from the rocket and studied to see if shearing will occur on any surfaces.
- Simulation #2, Landing LOW penetration Case #1: non-finned rover is simulated hitting the ground with low penetration to examine the occuring damage from a harsh impact force.
- Simulation #3, Landing HIGH penetration Case #1: non-finned rover is simulated hitting the ground with high penetration to examine the occuring damage from impacting with a soft surface such as sand or mud.
- Simulation #4, Ejection from Rocket Case #2: finned rover is simulated as ejecting from the rocket and studied to see if shearing will occur on any surfaces.
- Simulation #5, Landing LOW penetration Case #2: finned rover is simulated hitting the ground with low penetration to examine the occuring damage from a harsh impact force.
- Simulation #6, Landing HIGH penetration Case #2: finned rover is simulated hitting the ground with high penetration to examine the occuring damage from impacting with a soft surface such as sand or mud.

In real life, each rover model is packed snugly into a 5.38” diameter rocket casing with a 800 Ns thrust motor on the back. During the launch the rocket reaches a maximum altitude of ~1200 ft, at 500 ft in the rocket decent via parachute, the rover is ejected. Upon ejection, the 44” rover parachutes unfold and control is decent at 12.1 ft/s for each model before terminal landing.

1.3 Outline Changes

The original report outline consisted of only examining one model of rover and what stresses it would experience in the simulation. As time has progressed, the team has questioned if this model will be adequate for the actual testing or if an alternative model should be considered. Therefore, rather than focus on very complex simulations for just one model, two simpler sets of simulations will be examined, each with several areas of comparison. This will be more beneficial to the current progression of the project and will hopefully help the team reach their decision.

1.4 Simulation Specifics & Mathematical Modelling

The materials used in our analysis will consist of the plastic PLA and a aluminum-polyethylene pairing. As such, our model will be solid and coincide with the formulas for linear elasticity. This means that our strain will be fairly small and should be proportional to stress. Additionally, when loads are removed it will return to its original form excluding any damages the loads or impacts cause. The equation we will base our material properties on is

$$\sigma = \mathbf{D} \cdot \mathbf{B} \cdot \mathbf{d}$$

Where sigma is stress, B is the body force vector, is the displacement vector, and D is the elastic tensor. The dot product of B and d is the scalar strain on the body.

2. Problem Statement

2.1.

2.2. Geometry & Materials of Case #1

For Case #1, this rover model is constructed from four major structural component types, with multiple repeated components and layers. The four major component designations are;

1. The rover chassis top plate, consisting of three layers, visualized in **Fig.#55**
2. The rover chassis bottom plate, consisting of three layers, visualized in **Fig.#54**
3. The rover chassis side plate, consisting of three layers, visualized in **Fig.#56**
4. The rover supportive brackets, visualized in **Fig.#57**

2.2.1. Geometry Description for Case #1

The rover model for Case #1 is constructed out of four 0.11811” thick plates held together by four structural L-brackets. The drive base of this rover, although omitted for this analysis, is attached to the bottom plate. The bottom plate consists of three-layers and is 11.000 inches long, 4.567 wide and is again 0.11811 inches thick. This component consists of three identical profiled plates, two 0.020 inch thick

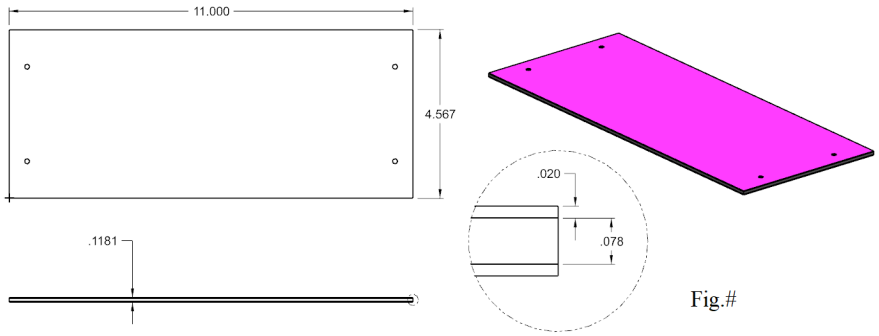

Fig.#

sandwiching one 0.078 inch thick core. The holes drilled into this plate would in reality provide a location for a bolt shank for securing the plate to the L-bracket supports, and in the simulation only serve as constraining references. This geometry can be visualized in **Fig.#54.**

Fig. #54: A visualization of the bottom chassis plate for Case #1.

The top plate of this rover model is nearly identical to the bottom plate, with only a differing width, 2.606 inches wide as compared to 4.567 inches wide. All layers follow the same profile, and the two holes have been omitted for the purposes of this analysis. This geometry may be visualized in **Fig.#55**.

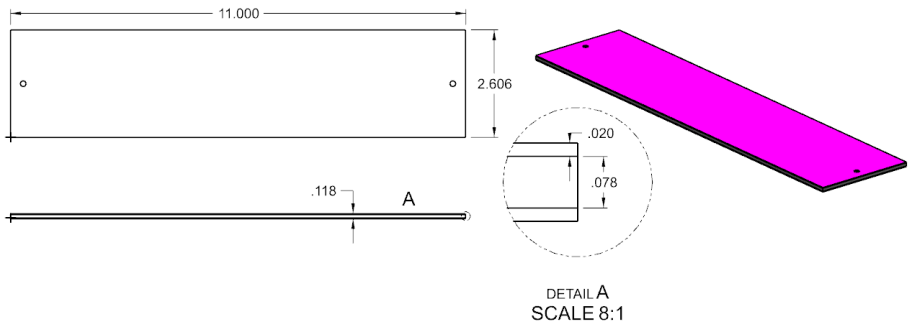

Fig.#55: A visualization of the top chassis plate for Case #1.

The side supporting chassi plates for the rover model for Case #1 have profiles with two straightaways and two connecting radii. They are 2.606 inches wide at the top, and 4.567 inches wide at the bottom with connecting radii of 3.250 inches. The layers carry the same profile and the top hole in

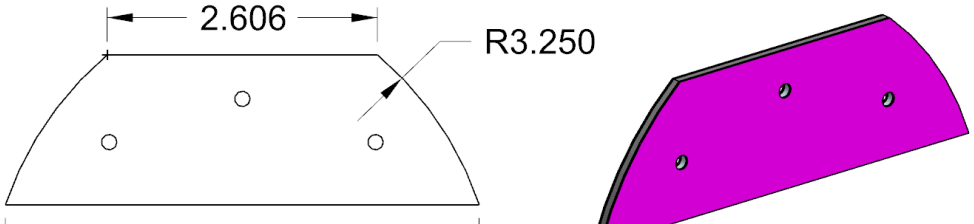

Fig.# will be omitted for this analysis. The two lower holes provide locations for a bolt shank for securing the plate to the L-bracket supports in real life, and in the simulation only serve as constraining references.

Fig.#56: A visualization of the side chassis plates.

Lastly, the rover model has four small supportive brackets. These bracket geometries are L-shaped with filleted faces, each face is 0.940 inches long on the outside (0.878 inches on the inside), 0.670 inches wide and 0.062 inches thick. Each face terminates in a 0.670 inch diameter half circle and has one 0.150 inch diameter hole drilled in each face center. The holes provide locations for a bolt shank for securing the L-bracket supports to the plate in real life, and in the simulation only serve as constraining references. This geometry may be viewed in **Fig.#57**.

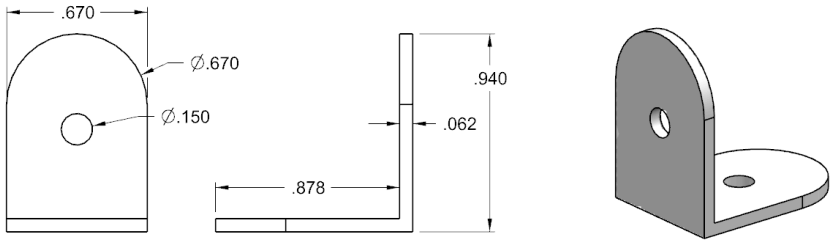

Fig.#57: A visualization of the dimensions & CAD of the supportive brackets.

2.2.2. **3D CAD Assembly Modelling of Case #1**

In terms of assembly, the bottom plate is secured to the two side plates via the four supportive brackets. Furthermore, the pink faces (as visualized in **Fig.#58**) of the side plates are adhered to all three

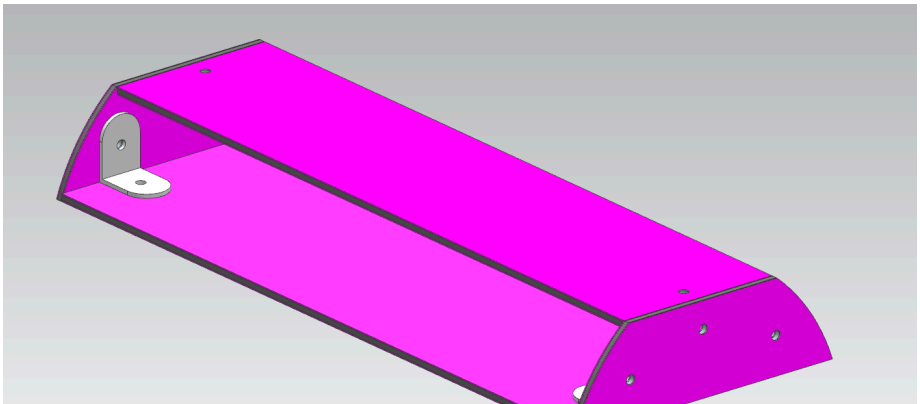

layers of the top plate. In real life, they would have been secured by two more brackets, however, for the sake of simplicity within this analysis, these brackets will be omitted.

Fig.#58: A visualization of the full 3D rover model for Case #1.

2.2.3. **Materials & Fabrication Details of Case #1**

For Case #1, the main chassis body plates and the supportive brackets consist of two different materials respectfully. The main chassis body plates were CNC routed from 0.11811” thick Durabond composite aluminum paneling, of which there are two 0.020” thick plates of 6061 aluminum sheets adhered to a 0.781” thick sheet of polyethylene. The polyethylene utilized in this paneling has a Young’s Modulus of 1.25 GPa, a poisson's ratio of 0.46, a density of 0.96 g/cm^3 and an ultimate tensile strength of 31.7 GPa. Furthermore, the 6061 series aluminum utilized in this composite paneling has a Young’s Modulus of 68.9 GPa, a poisson's ratio of 0.33, a density of 2.71 g/cm^3 and an ultimate tensile strength of 310GPa. The supportive brackets were also constructed out of 6061 series aluminum, so the same material properties will be run. Due to a lack of consistency in the stress-strain data for the materials in Case #2, these materials will be simulated as perfectly elastic.

2.3. **Boundary Conditions of Case #1**

2.3.1. Rocket Ejection for Case #1 [Simulation #1]

For running Sim.#1 with Case #1, the rover is being ejected out of a 5.380 inch diameter rocket body via two ejection charges issuing a maximum of 15 psi back pressure of which correspondingly forces the rover out. Being that this event occurs over such a small period of time (0.005 s), a fixed constraint will be placed on the face farthest opposing the pressurized face to clearly illustrate the desired moment of compression before rover ejection motion begins.All other degrees of freedom are unconstrained to allow for Y, and Z deformation, however being that the rover deformation is contained

within a 5.38 inch rocket body, the ending simulation will be studied for realism. These boundary conditions may be visualized in **Fig.#59.**

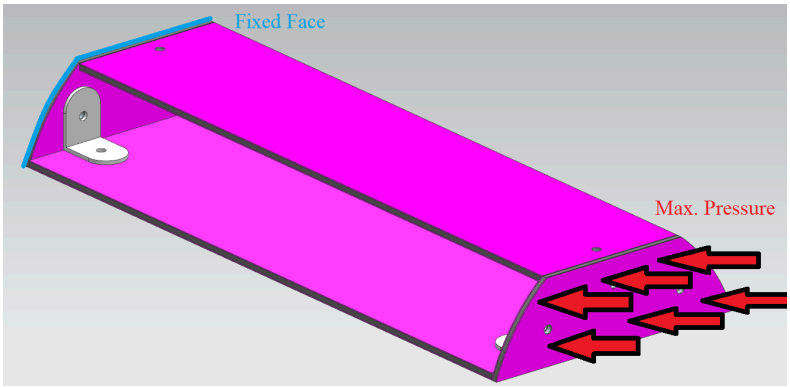

Fig.#59: A visualization of the Sim.#1 boundary conditions.

In terms of simulation object relationships, there are a total of 18 relationships,however, condensed, they are;

1.) The two top chassis plates experience a Surface to Surface Glue relationship to the middle polyethylene core.
2.) The two side chassis plates each experience a Surface to Surface Glue relationship to the middle polyethylene cores for both full side chassis plates.
3.) The bottom chassis plates experience a Surface to Surface Glue relationship to the middle polyethylene core.
4.) Each of the two faces of all four supportive brackets experience a Surface to Surface Glue relationship to each respective chassis surface plate of which may be seen in **Fig.#60.**
5.) The bottom chassis plate edges as indicated in **Fig.#61** in light green experience Surface to Surface Contact relationships with a friction coefficient of 0.25 [2].

6.) The top chassis plate edges experience a Surface to Surface Glue relationship to each respective chassis surface plate of which may also be seen in **Fig.#61.**

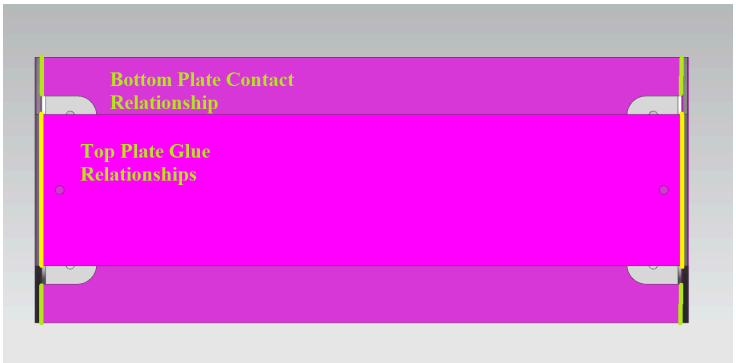

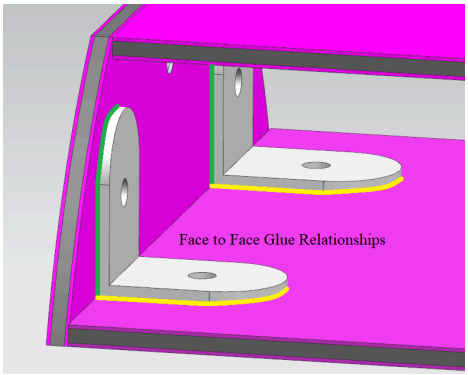

Fig.#61: A visual of the top and bottom plate relationships **Fig.#60:**: A visual of the bracket relationships

2.3.2. Rover Landing with LOW Penetration for Case #1 [Simulation #2]

Sim.#2 will be modelling the landing of the Case #1 rover with one 44" parachute onto a ground substrate with very low penetration. The hard ground substrate in this instance would be finely packed dirt that, with the rover landing, would only allow 0.125" of penetration in the Z-direction, and 3.000" (observed experimentally) of skidding penetration in the perpendicular direction. The manner in which the rover is held by the parachute lines fully dictates the manner in which this particular rover model will fall - this model rover will be landing on the leading edge of the left hand face as indicated in **Fig.#62** on an angle of approximately 20 degrees off vertical**.** Assuming 10mph horizontal air flow (4.47 m/s) in conjunction with an estimated fall speed of 8.25mph (3.688 m/s) (due to previous parachute calculations), and this rover model having a mass of 1425 grams with all loaded electronics and additional components, the calculations for impact force follow thusly;

$$F_{max} = \frac{m(v^2)}{(\Delta d)}$$

$$F_{max,x} = \frac{(1.425\ kg)(4.47\frac{m}{s})^2}{0.0762\ m} = 373.659\ N$$

$$F_{max,y} = \frac{(1.425\ kg)(3.688\frac{m}{s})^2}{0.003175\ m} = 6104.54\ N$$

In order to simulate this impact force, this F_{max} will be broken up into $F_{x'}$ and $F_{y'}$ according to the corresponding components of velocity adjusted for the angle of impact of the rover. Accordingly, the F_x force applied is 351.12 N, and the F_y force applied will be 5736.39 N.

All object simulation relationships detailed in Sim.#1 will be identical for Sim#2.

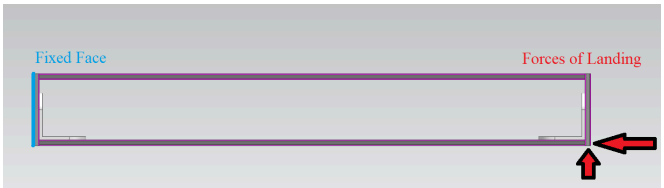

Fig.#63: A visual of landing loads & constraints for Sim.#2 & #3.

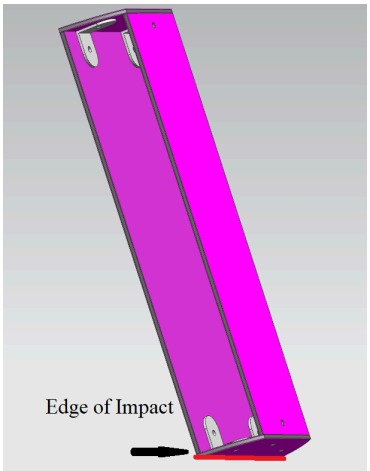

Fig.#62: A visual of the edge of impact for the Case #1 model.

2.3.3. Rover Landing with HIGH Penetration for Case #1 [Simulation #3]

Sim.#3 will be modelling the landing of the Case #1 rover with one 44" parachute onto a ground substrate with very high penetration. The softer ground substrate in this instance would be a wet muddy substrate that, with the rover landing, would allow 1.500" of penetration in any direction. The manner in which the rover is held by the parachute lines fully dictates the manner in which this particular rover model will fall - this model rover will be landing on the leading edge of the left hand face as indicated again in **Fig.#62** on an angle of approximately 20 degrees off vertical**.** Assuming 10mph horizontal air flow (4.47 m/s) in conjunction with an estimated fall speed of 8.25mph (3.688 m/s) (due to previous parachute calculations), and this rover model having a mass of 1425 grams with all loaded electronics and additional components, the calculations for impact force follow thusly;

$$F_{max} = \frac{m(v^2)}{(\Delta d)}$$

$$F_{max,x} = \frac{(1.425\ kg)(4.47\frac{m}{s})^2}{0.0381\ m} = 747.317\ N$$

$$F_{max,y} = \frac{(1.425\ kg)(3.688\frac{m}{s})^2}{0.0381\ m} = 508.712\ N$$

In order to simulate this impact force, this F_{max} will be broken up into F_x, and F_y, according to the corresponding components of velocity adjusted for the angle of impact of the rover. Accordingly, the F_x force applied is 702.248 N, and the F_y force applied will be 478.033 N. These individual boundary conditions may be visualized again in **Fig.#63**, only with differing force magnitudes.

All object simulation relationships detailed in Sim.#1 will be identical for Sim#3.

2.4. Geometry & Materials of Case #2

For Case #2, this rover model is constructed from four major structural components;

1. The main rover chassis, visualized in **Fig.#1** and **Fig.#2**.
2. The rover chassis cover, visualized in **Fig.#3** and **Fig.#4**.
3. The top rover flipper, visualized in **Fig.#5**.
4. The bottom rover flipper, identical to the top flipper, also visualized in **Fig.#5**.

2.4.1. Geometry Description for Case #2

The main rover chassis, visualized in **Fig.#1** and **Fig.#2**, is the main force bearing structure of the Case #2 rover model. This geometry is best described as a shell supporting the necessary servos, flippers and corresponding electronics, as well as the lines connecting to the main rover parachute. The main chassis has an overall length of 10.562 inches, a width of 3.828 inches and a depth of 2.125 inches with two servo supportive features on either end and both a battery compartment (0.992 inches by 5.563 inches in **Fig.#1**) and electronics compartment space. The two servo supportive features at either end of this main chassis would each contain two 55 gram MG995 modified servos of which would operate the flipper rotation motion, each servo features are 2.953 inches long by 0.875 in width and 2.000 inches in depth. In addition, with a shell thickness of 0.188 inches (3/16”), the main chassis has an off center notch to accommodate for one servo spinning a dirt collecting cammed scoop not pictured and not included within this analysis. The notch however, is 1.312 inches in width from outside edge to outside edge, 4.668 inches in length and begins 1.500 inches from the bottom leading edge.

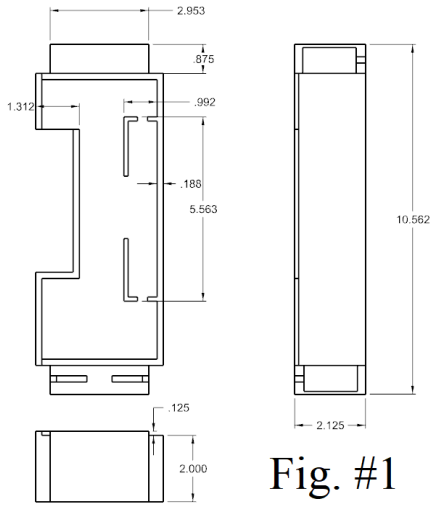

Fig. #1

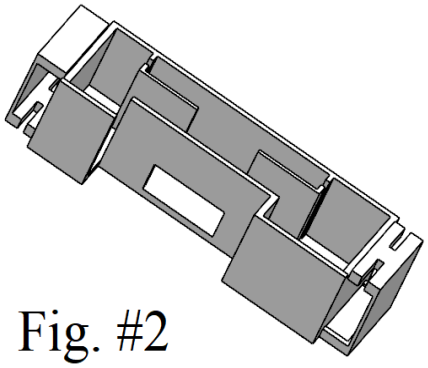

Fig. #2

Fig.#1: A drafting of the main rover chassis.

Fig.#2: A 3D visualization of the main rover chassis

The main chassis cover, again visualized in **Fig.#3** and **Fig.#4**, is a 0.125 inch (⅛”) thick plate capturing the dimensions of the main chassis in order to contain and protect the critical electronics as well as to give the top leading edge of the main chassis support for both the forces of ejection as well as for landing. This plate has 0.125 inch diameter holes at strategic positions, however, for the purposes of this analysis these holes will not be load bearing as the corresponding threaded flanges on the main rover chassis have been removed for simplicity. The overall dimensions if this plate geometry are 8.812 inches long, 3.640 inches wide with an off-center notch beginning 1.500 inches up from the bottom leading edge that is 1.125 inches in width and 4.688 inches in length as can be visualized in **Fig.#3**.

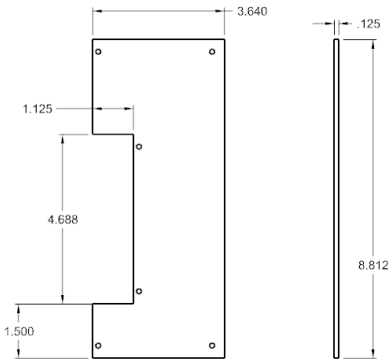

Fig. #3

Fig.#3: A drafting of the rover cover.

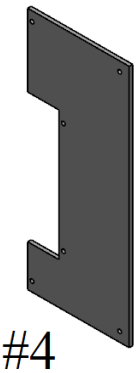

Fig. #4

Fig.#4: A 3D visualization of the rover cover.

Lastly, the two top and bottom flippers that provide the locomotion of this rover model, as identically visualized in **Fig.#5**, are 0.188 inch thick (3/16”) flanged plates. These flanged plates have weight saving grooves in the physical construction, however, for this analysis, these grooves will be omitted. In box dimensions, the overall length of this geometry is 7.500 inches, 1.438 inches in depth with an overall width of 4.375 inches to easily fit around the locomotive servos held in the main rover chassis. The side flanges that translate the servo torque to the bottom plate have a unique geometry in order to provide both servo and chassis clearance, this side profile dimensions may be visualized in **Fig.#5**.

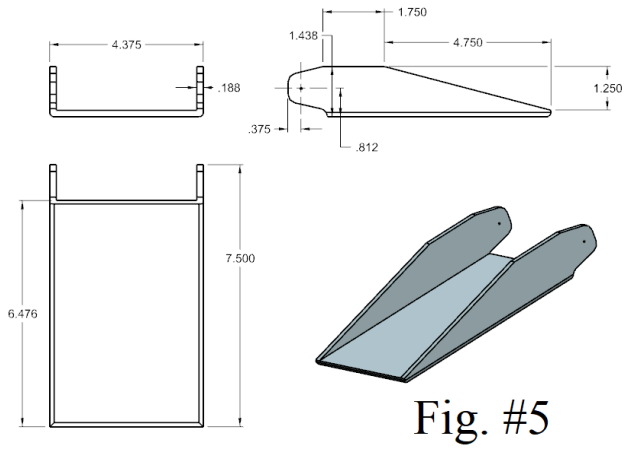

Fig. #5

Fig.#5: A drafting and 3D visualization of the rover flipper (2X)

2.4.2. **3D CAD Assembly Modelling of Case #2**

In terms of model assembly for Case #2, the main rover cover in **Fig.#4** fits up and over on to the 'top' of the main rover chassis as detailed in **Fig.#6** and **Fig.#7** and is constrained via alignment due to the absence of threaded flanges. Additionally, the two flippers are constrained in the position they would be in if the locomotive servos were in place, this real life situation may be seen in **Fig.#8**. However, during

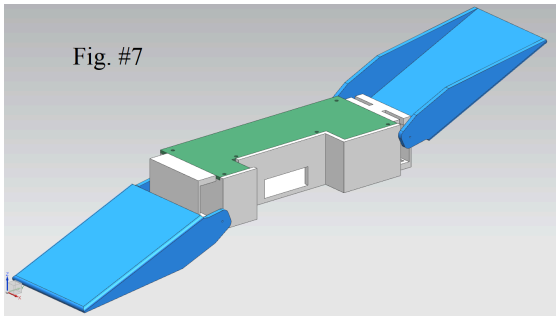

the simulation, it was deemed necessary to omit the flippers from the assembly to accurately model the acting pressures on the main chassis.

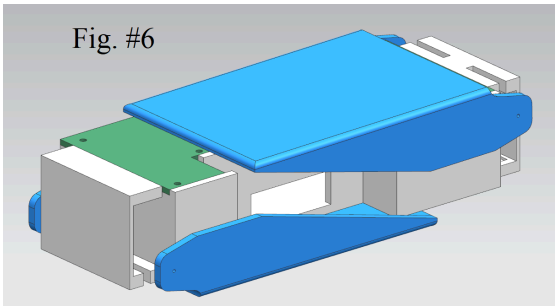

Fig.#6: A 3D visual of the Case #2 closed assembly. **Fig. #7:** A 3D visual of the Case #2 open assembly.

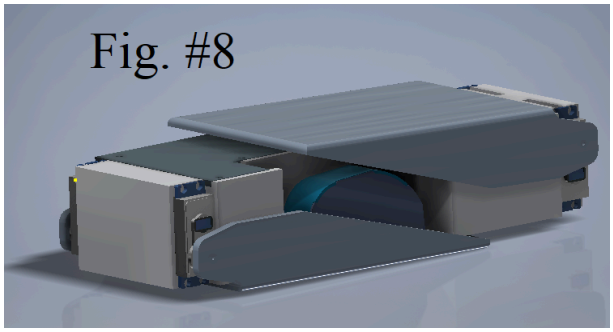

Fig.#8: A 3D model of Case #2 with all omitted components and features.

2.4.3. **Materials of Case #2**

For Case #2, for the four main components all consist of the same 3D-printed high resolution polylactic acid (PLA) material with a Young's Modulus of 3.5 GPa, an ultimate tensile strength of 35 GPa, Poisson's Ratio of 0.33 and a density of 1.25 g/cm^3 [1]. This material will be run as a linear elastic material due to a distinct lack of reliable strain-stress relationship data.

2.5. **Boundary Conditions of Case #2**

2.5.1. Rocket Ejection for Case #2 [Simulation #4]

For running simulation #4 with Case #2, the ejection of the rover occurs during a receptively short timespan, and during this time, the pressure from the gunpowder ejection charge issues a maximum

of a 15 psi back pressure of which correspondingly forces the rover out. This pressure will be placed on the left hand back face of the servo support feature as visualized in **Fig.#10**. For Sim.#4, a fixed constraint will be placed on the opposing servo support feature again indicated in **Fig.#10**, in order to model the

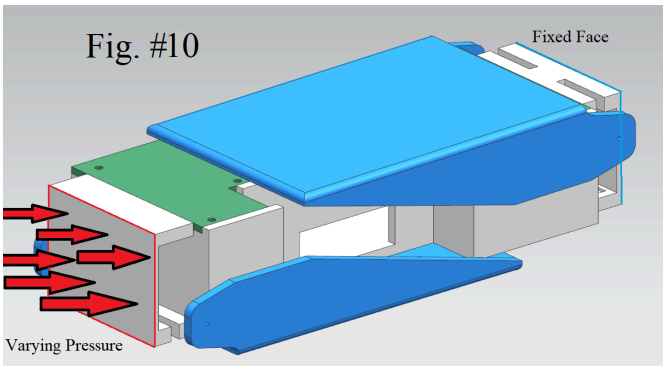

moment of desired compression phenomenon before the rover begins significant motion. All other degrees of freedom are unconstrained to allow for Y, and Z deformation, however being that the rover deformation is contained within a 5.38 inch rocket body, the ending simulation will be studied for realism.

Fig.#10: A visual of Sim.#4 loads & constraints.

In terms of simulation object relationships, Sim.#4, there are four object relationships:

1. The visually green rover cover is glued to all bottom contacting faces on the main rover chassis via a Surface to Surface Glue relationship.

2. The visually blue top flipper plate face experiences a Surface to Surface Contact relationship with a PLA to PLA friction coefficient of 0.40 with the green rover cover and the top regions of the main rover chassis [3].

3. The visually blue bottom flipper plate face experiences a Surface to Surface Contact relationship with a PLA to PLA friction coefficient of 0.4 with the bottom face of the main rover chassis [3].

4. The visually green rover cover experiences a Surface to Surface Contact relationship with a PLA to PLA friction coefficient of 0.4 on all adjacent main chassis faces [3].

Note: Relationships 2 & 3 have been omitted along with the flipper bodies for simulation clarity.

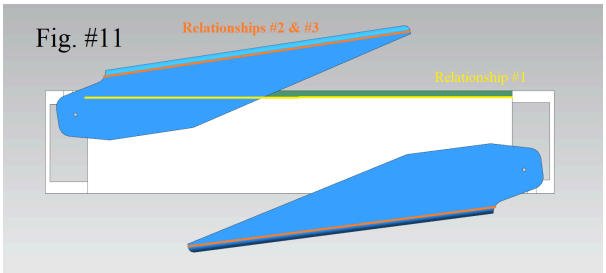

Fig. #11: A visualization of object simulation relationships #1-3.

2.4.2 Rover Landing with LOW Penetration for Case #2 [Simulation #5]

Sim.#5 will be modelling the landing of the Case #2 rover with one 44" parachute onto a ground substrate with very low penetration. The hard ground substrate in this instance would be finely packed dirt that, with the rover landing, would only allow 0.125" of penetration in the Z-direction, and 3.000" (observed experimentally) of skidding penetration in the perpendicular direction. The manner in which the rover is held by the parachute lines fully dictates the manner in which this particular rover model will fall - this model rover will be landing on the leading edge of the left hand face as indicated in **Fig.#12** on an angle of approximately 25 degrees off vertical**.** Assuming 10mph horizontal air flow (4.47 m/s) in conjunction with an estimated fall speed of 8.25mph (3.688 m/s) (due to previous parachute calculations), and this rover model having a mass of 1257 grams with all loaded electronics and additional components, the calculations for impact force follow thusly;

$$F_{max} = \frac{m(v^2)}{(\Delta d)}$$

$$F_{max,x} = \frac{(1.257\ kg)(4.47\frac{m}{s})^2}{0.0762\ m} = 329.606\ N$$

$$F_{max,y} = \frac{(1.257\ kg)(3.688\frac{m}{s})^2}{0.003175\ m} = 5384.847\ N$$

In order to simulate this impact force, this F_{max} will be broken up into $F_{x'}$ and $F_{y'}$ according to the corresponding components of velocity adjusted for the angle of impact of the rover. Accordingly, the F_x force (Force #2) applied is 298.725 N, and the F_y force (Force #1) applied will be 4423.18 N. These

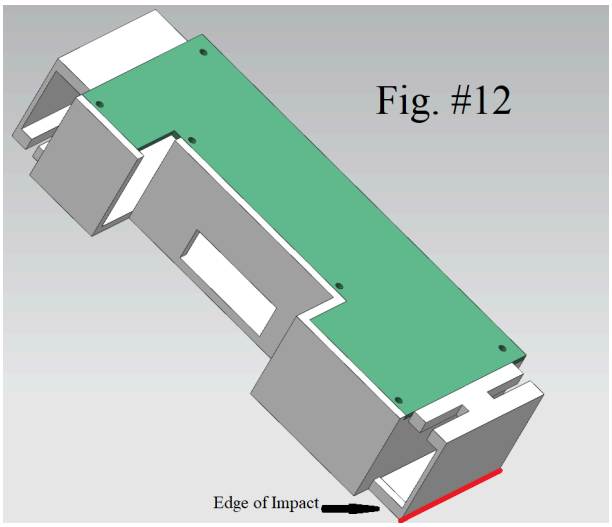

individual boundary conditions may be visualized in **Fig.#13** with the two applied edge forces and the opposing face fixed.

Fig.#12: Visualization of the impact edge of Case #2 for Sim.#5 & Sim.#6

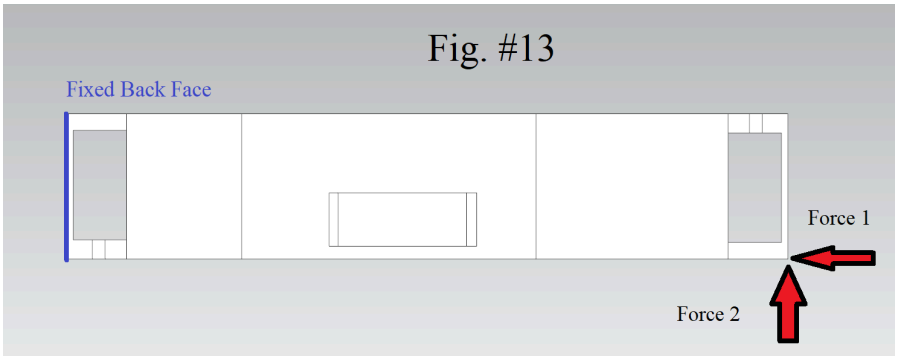

Fig.#13: Visualization of applied boundary conditions for Case #2 for Sim.#5 & Sim #6

All object simulation relationships detailed in Sim.#4 will be identical for Sim#5.

2.4.3 Rover Landing with HIGH Penetration for Case #2 [Simulation #6]

Sim.#6 will be modelling the landing of the Case #2 rover with one 44" parachute onto a ground substrate with very high penetration. The softer ground substrate in this instance would be a wet muddy substrate that, with the rover landing, would allow 1.500" of penetration in any direction. The manner in which the rover is held by the parachute lines fully dictates the manner in which this particular rover model will fall - this model rover will be landing on the leading edge of the left hand face as indicated again in **Fig.#12** on an angle of approximately 25 degrees off vertical**.** Assuming 10mph horizontal air flow (4.47 m/s) in conjunction with an estimated fall speed of 8.25mph (3.688 m/s), the velocity magnitude will be again 12.95mph (5.788 m/s). Being that this rover model with all onboard electronics and additional components has a mass of 1257 grams and is de-accelerating from 5.788 m/s over 1.500" (0.0381m);

$$F_{max} = \frac{m(v^2)}{(\Delta d)}$$

$$F_{max,x} = \frac{(1.257\ kg)(4.47\frac{m}{s})^2}{0.0381\ m} = 659.213\ \text{N}$$

$$F_{max,y} = \frac{(1.257\ kg)(3.688\frac{m}{s})^2}{0.0381\ m} = 448.737\ \text{N}$$

In order to simulate this impact force, this F_{max} will be broken up into $F_{x'}$ and $F_{y'}$ according to the corresponding components of velocity adjusted for the angle of impact of the rover. Accordingly, the F_x force applied is 597.45 N, and the F_y force applied will be 406.694 N. These individual boundary conditions may be visualized again in **Fig.#13** with the two applied edge forces and the opposing face fixed, however the given forces, #1 and #2, are now 406.694 N and 597.45 n respectively.

All object simulation relationships detailed in Sim.#4 & Sim.#5 will be identical for Sim#6.

3. Analysis

3.1. Convergence Analysis

The mesh element size was selected between 0.01 and 2.4 because our team part was so complex. The simulation has a difficult time running if the mesh size were more uniform and all equally small. Additionally, the pieces were not always made of uniform material, nor had uniform thickness. It would have been more ideal to use a uniform mesh for a 2D model, but because of our parts a non-uniform mesh size worked better in this case. Mesh uniformity would have been more important if more curved pieces had been incorporated, but this was not the case. It is worth noting, that Simulations #1 through #3 had difficulties running due to convergence not being reached after 1000 iterations for each force loop using the element iterator solver, thus there is some minute error involved with those respectful simulations.

3.2. Problem Analysis

Characteristic	**Simulation 1**	**Simulation 4**
Mesh Size	0.015350 - 0.141336 in	0.011554 - 0.242158 in

Max Displacement	0.0010938 in	0.0171 in
Location of Max Displacement	10,967, the top plate	32,861 (Impact face)
Max Shear	12.22 MPa	6.42 MPa
Location of Max Shear	45,779, back of the impact face	60,930, Impact face corner
Worst Principal Stress	20.78 MPa	9.11 MPa

Characteristic	**Simulation 2**	**Simulation 3**	**Simulation 5**	**Simulation 6**
Mesh Size	0.015350 - 0.141336 in	0.015350 - 0.141336 in	0.011554 - 0.242158 in	0.011554 - 0.242158 in
Max Displacement	0.23767 in	0.52951 in	0.143973 in	0.467683 in
Location of Max Displacement	Entire impact face experienced ~0.2377 in deformation	Entire impact face experienced ~0.5295 in deformation	33,324, bottom left of impact edge	33,324, bottom left of impact edge
Max Shear	238.50 MPa	539.09 MPa	28.28 MPa	47.94 MPa

Location of Max Shear	45,780, contact point between the top and the side panels	45,780, contact point between the top and the side panels	105,728, a corner on the back face	68,964, a corner on the back face
Worst Principal Stress	351.63 MPa	790.05 MPa	40.10 MPa	1156.93 MPa

3.3. Simulation #1 Result Imaging

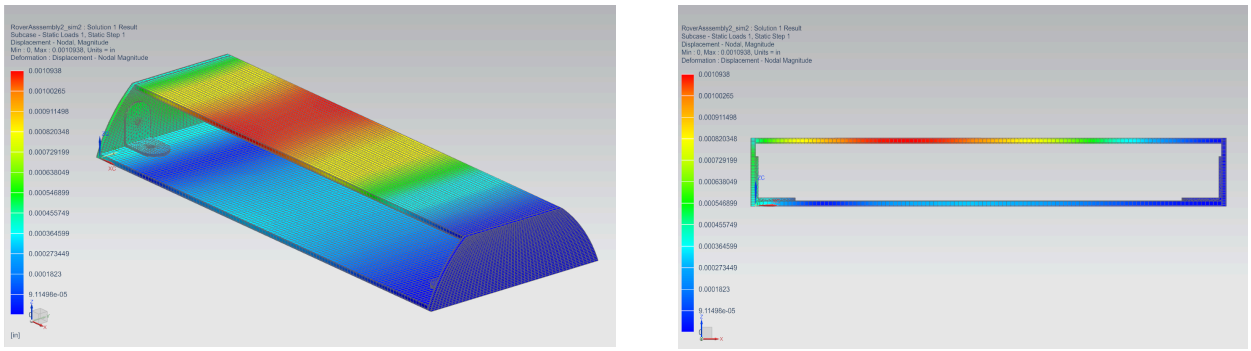

Fig.#14 & 15: Max Displacement, Sim #1, Case #1

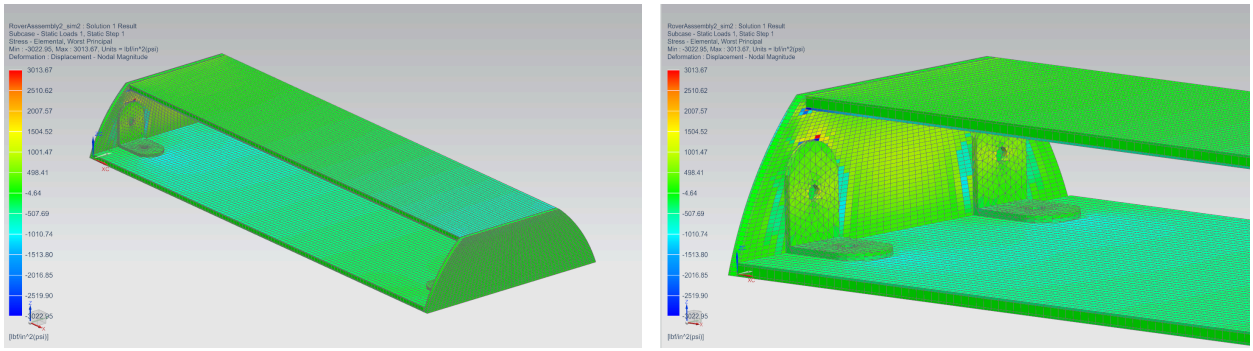

Fig.#16 & 17: Worst Principal Stress, Sim #1, Case #1

Fig.#18 & 19: Max Shear, Sim #1, Case #1

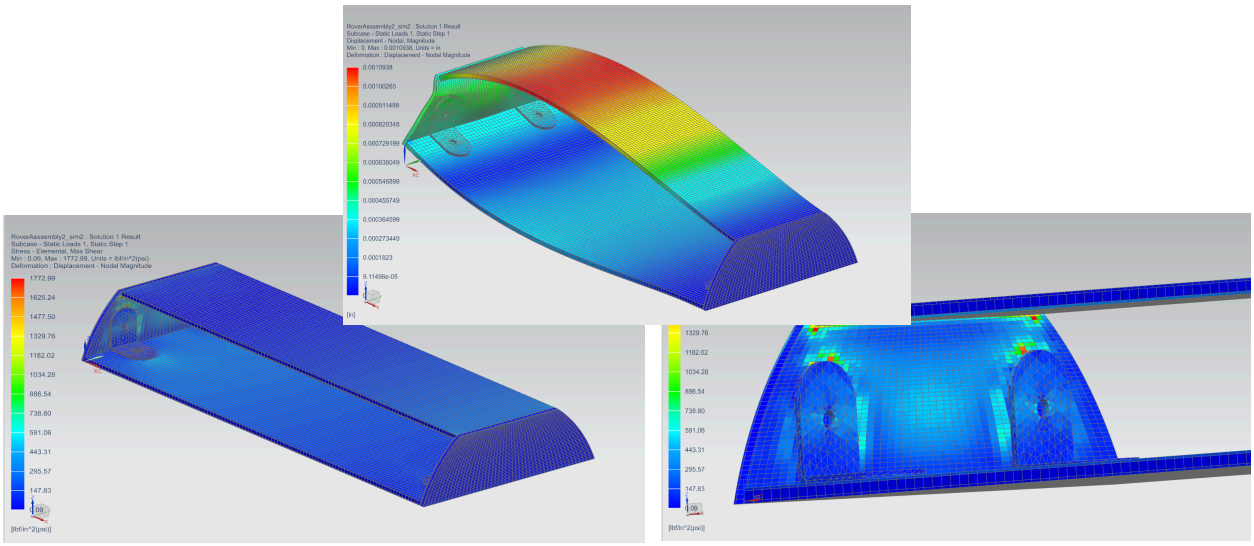

Fig.#20: Exaggeration of bowing from Ejection, Sim #1

3.4. Simulation 2 Result Imagining

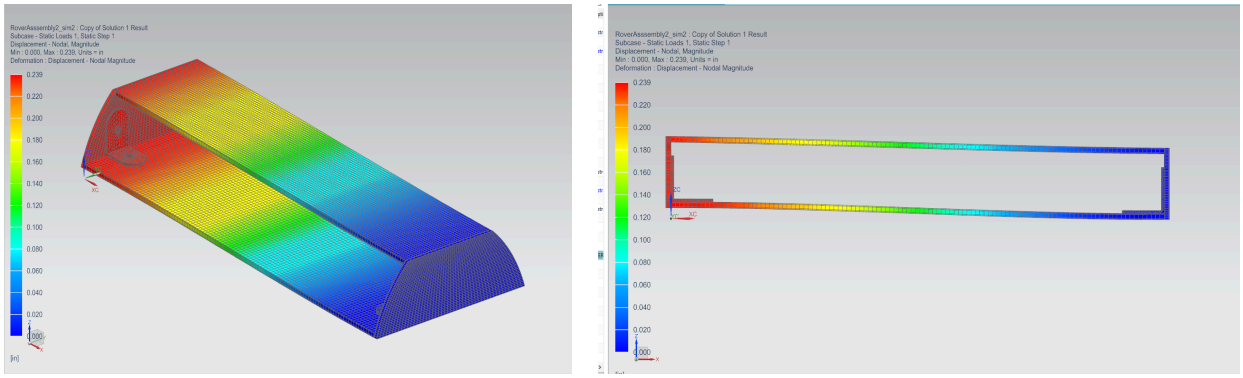

Fig.#21 & 22: Max Displacement, Sim #2

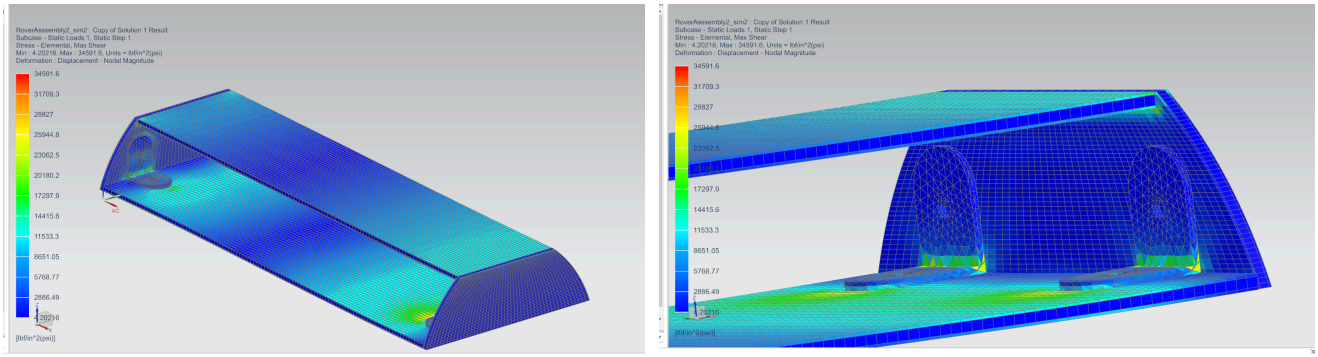

Fig.#23& 24: Max Shear, Sim #2

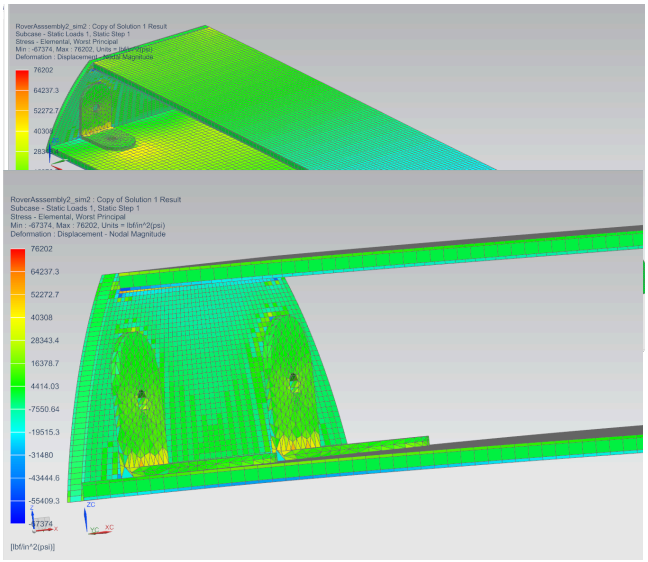

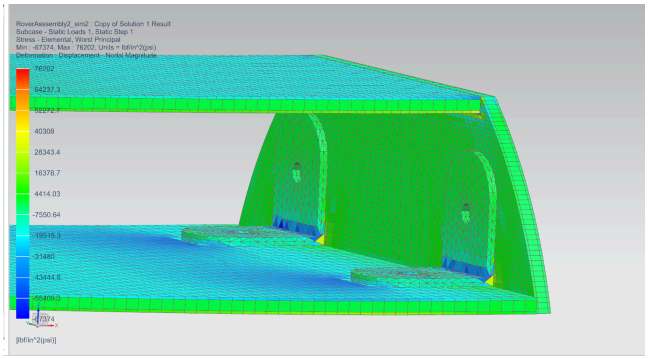

Fig.#25, 26 & 27: Worst Principal Stress, Sim #2

3.5 Simulation 3 Result Imagining

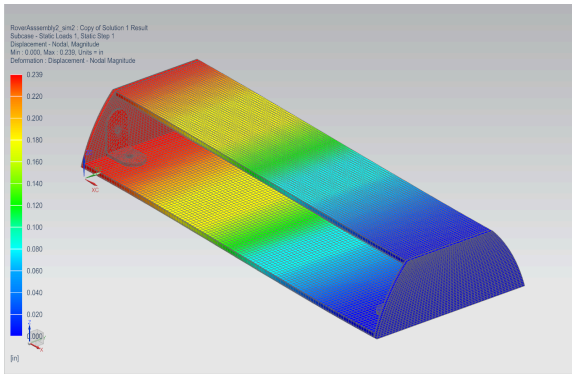

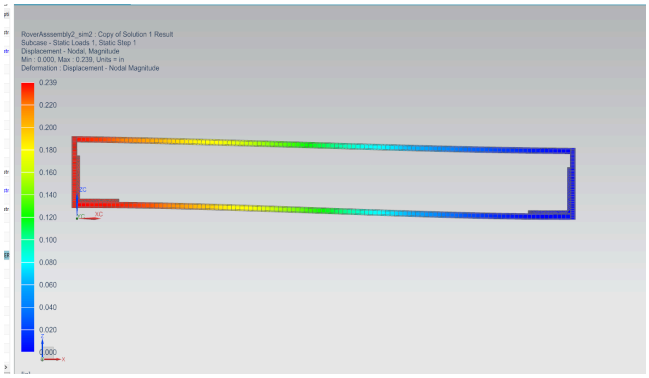

Fig.#28 & 29: Max Displacement, Sim #3

Fig.#30, 31 & 32: Max Shear, Sim #3

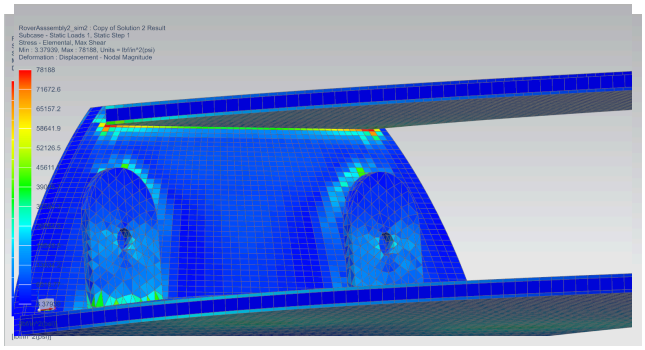

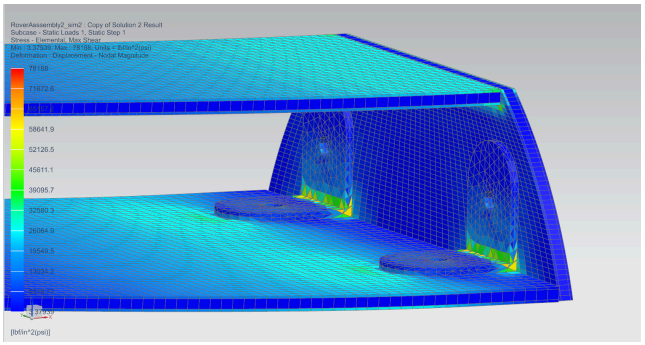

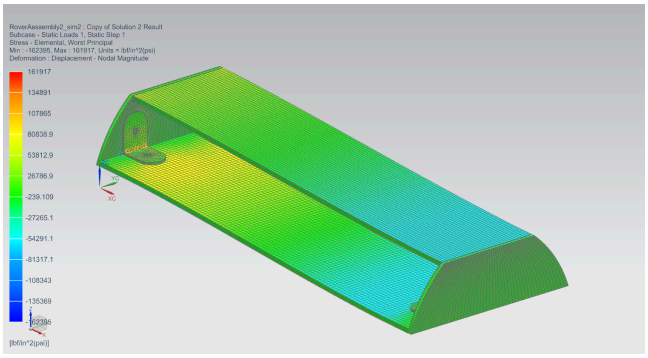

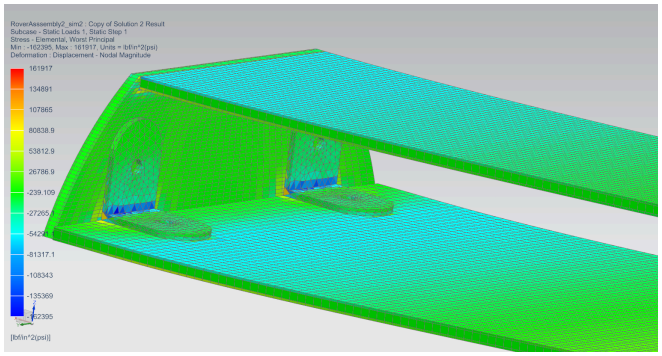

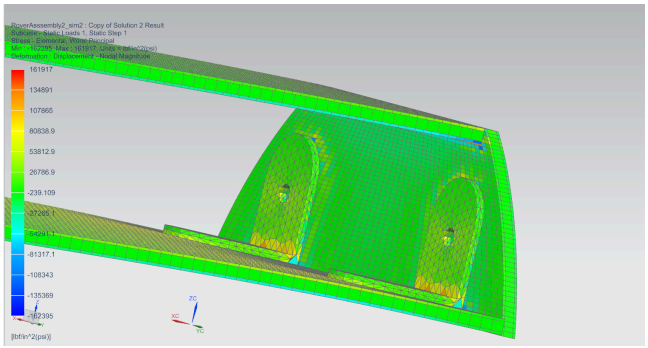

Fig.#33, 34 & 35: Worst Principal Stress, Sim #3

3.6. Simulation 4 Result Imagining

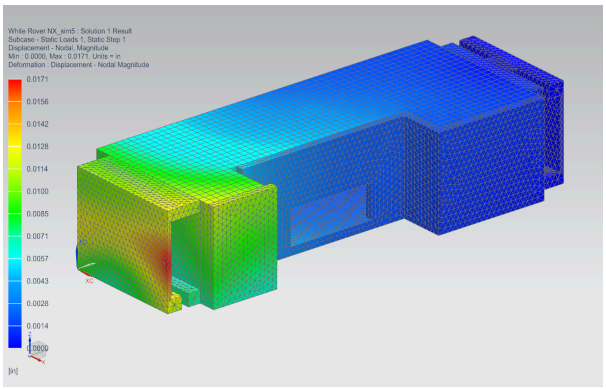
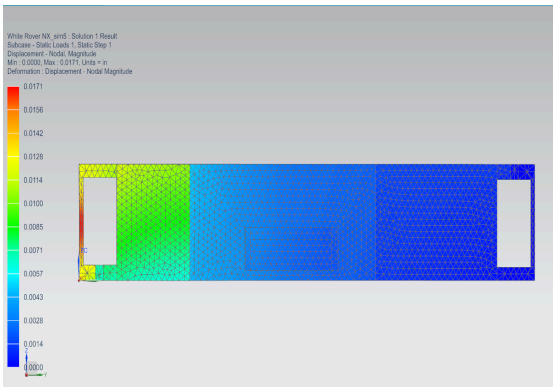

Fig.#36 & 37: Max Displacement, Sim #4

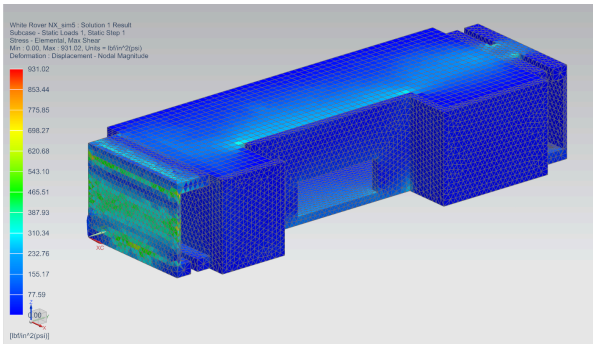
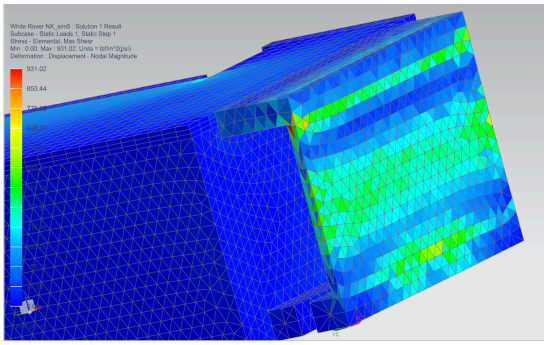

Fig.#38 & 39: Max Shear, Sim #4

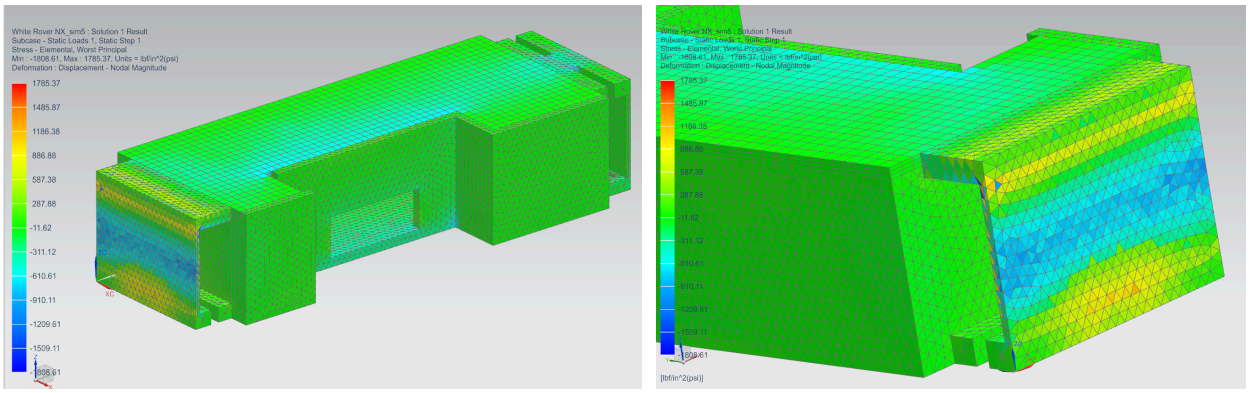

Fig.#40 & 41: Worst Principal Stress, Sim #4

3.7. Simulation 5 Result Imaging

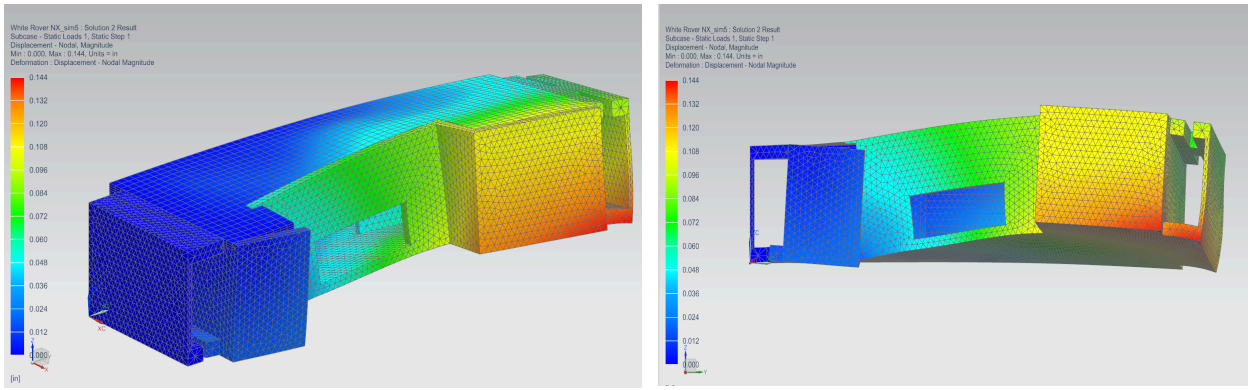

Fig.#42 & 43: Max Displacement, Sim #5

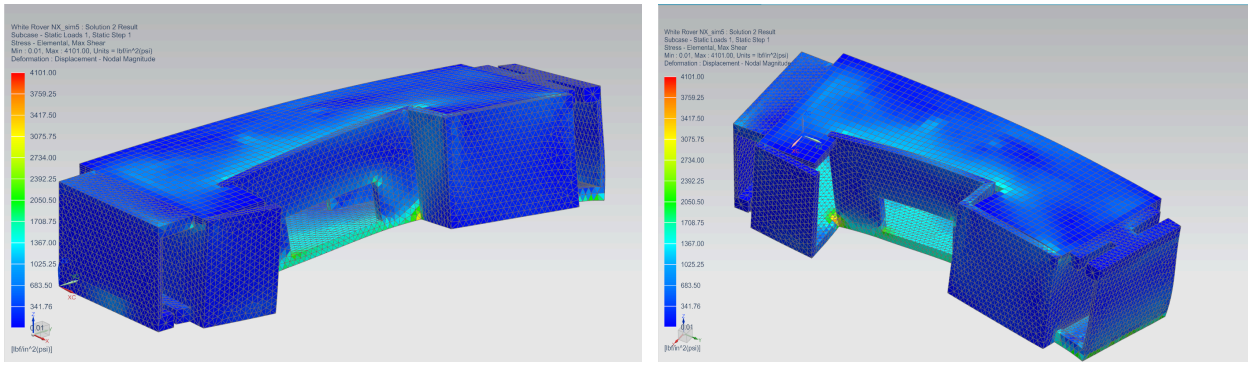

Fig.#44 & 45: Max Shear, Sim #5

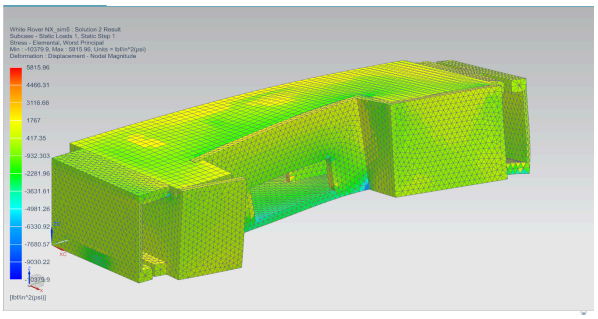

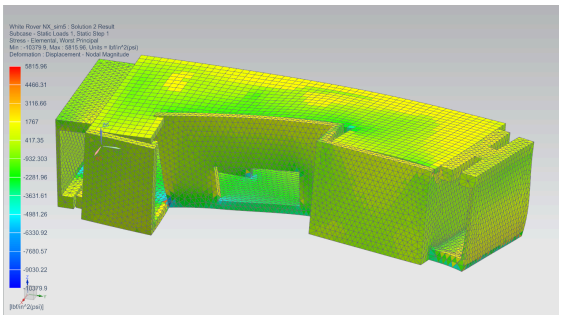

Fig.#46 & 47: Worst Principal Stress, Sim #5

3.8. Simulation 6 Result Imaging

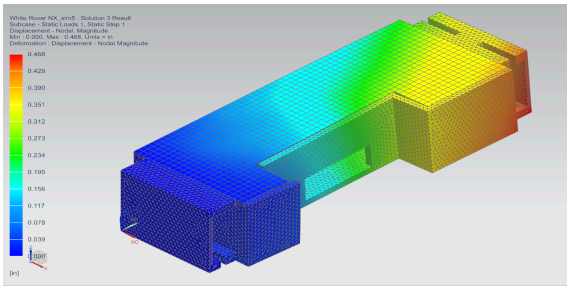

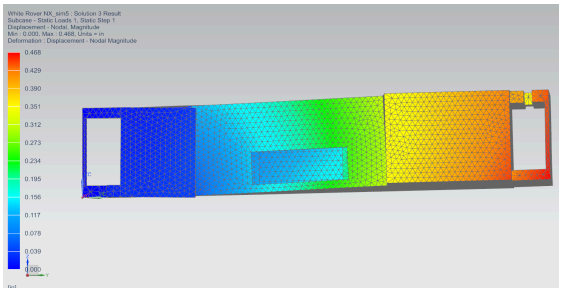

Fig.#48 & 49: Max Displacement, Sim #6

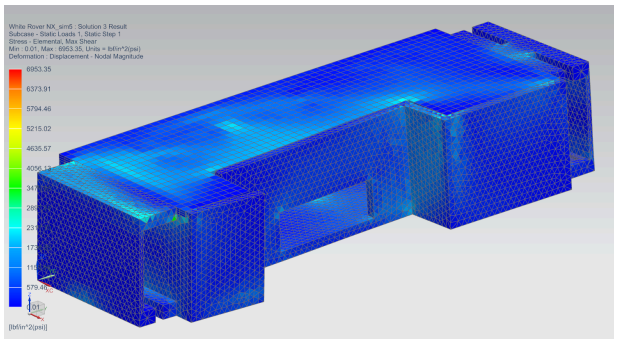

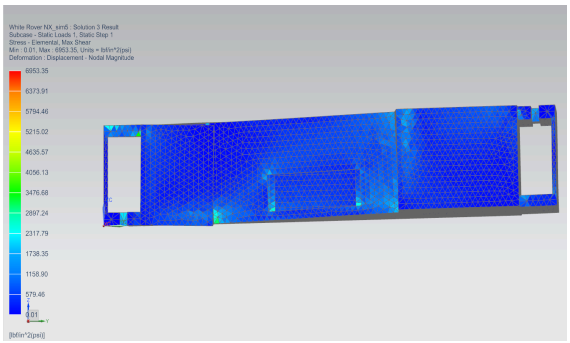

Fig.#50 & 51: Max Shear, Sim #6

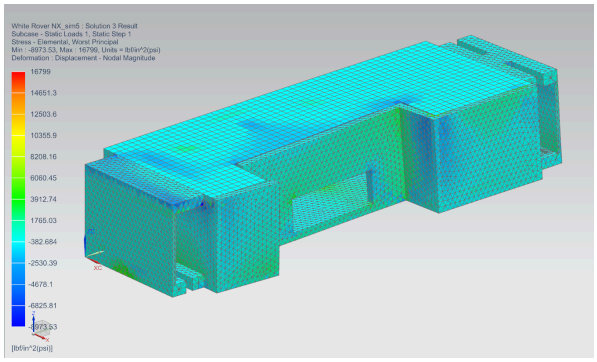

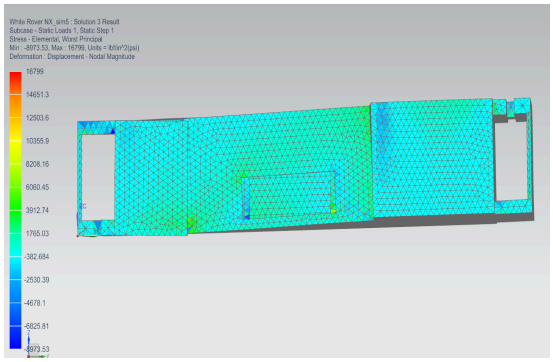

Fig.#52 & 53: Worst Principal Stress, Sim #6

4. Results and Discussion

4.1. Simulation 1

For the first simulation, we see that the maximum displacement in Figures 14 and 15 does not occur on the surface where the force is exerted. Rather, max displacement is in the middle of the piece, where the walls are more prone to buckling. The force exerted on one side and the reaction from the other cause a bending towards the center that is best depicted in Figure 20. Maximum shear, depicted in Figures 18 and 19, is at the upper edges of the braces, where the material is able to rub against the body because it is not constrained at the very top. The worst principal stress, shown in FIgures 16 and 17, is also centered around the braces, indicating areas where the ejection took the greatest toll on the body.

4.2. Simulation 2

The displacement for Simulation 2 in Figures 21 and 22 is centered on the side where impact occurred and continues to roll across the body. The shearing of Figures 23 and 24 occurs heavily at the joints of the brackets because the bottom face wants to be forced backwards relative to the perpendicular impact face. The worst principal stresses in Figures 25, 26, and 27 also occur in this area, but only on the brackets on the impact side that are struggling to keep the bottom plate from actually moving.

4.3. Simulation 3

Since Simulation 3 is another impact analysis, it is expected to have many of the same results that simulation 2 produced. This is indeed the case as we can see from our simulation depictions, but with the difference of values. Simulation 3 is the higher impact and so has a greater amount of displacement, principal stresses, and shear. It can be noted though that the shear has become so great it has begun to

affect the upper parts of the bracket that is having difficulty keeping the lower plate in place and wants to slide down the perpendicular wall.

4.4. Simulation 4

The displacement, shear, and stress of Simulation 4 are on a completely new body, one with more material. Therefore, the greatest amount of all three occur on the face where the ejection force was exerted. More notably for shear it occurs in the center of the face where there is the least material. For worst stress, it occurs along the edge of the face where there is more material to push at.

4.5. Simulation 6

For the high impact of simulation 6, we can see that there is displacement on an angle because the piece impacts the ground on an angle. This also leads to some slight twisting of the piece. Because of the twist, the max shear occurs on the side that is nearly parallel to the ground and is worst at the bottom meeting of the parallel and perpendicular inside faces. The principal stresses are spread all over the body in a seemingly non-uniform pattern.

4.6. Simulation 5

Simulation 5 carries many of the same results as simulation 6, but on a lesser sale because of the lower impact. Displacement occurs in a similar shape, stresses are extremely similar, and shear is a little more centered towards the back of the piece.

4.7. Simulation 1 vs. 4

Simulations 1 and 4 both have their trade offs because of their designs and the amounts of material used. 4 has the greatest displacement and will have a decent amount of deformation, but the shear

and stress on 1 are nearly 4 times larger. The fact that this does not severely impact the displacement of the model is a good sign. It shows that the brackets are handling the forces efficiently.

4.8. Simulation 2 vs. 5

The maximum displacement for impact is found in simulation 2. Additionally, simulation 2 has the greater shear and max principal stresses. Despite this, the displacement of 2 is only 2 times greater than that of 5. Both pieces under a low impact situation do not appear to suffer greatly, but the conditions of 5 are such that it would have broken.

4.9. Simulation 3 vs. 6

Simulation 3 and 6 is similar in comparison to 2 and 5, except that simulation 6 has a shear greater than 3 that would have definitely caused the piece to break.

4.10. Simulation 2 vs. 3

Both 2 and 3 experienced the expected similar impact results, but the fact that the material is more able to bend long the top face may have saved it from overall design failure. The brackets help to distribute the forces and stresses in such a way that keep the part mostly contained.

4.11. Simulation 5 vs. 6

The stresses in simulation 5 and 6 are such that although both pieces would have broke, the higher simulation would have been much worse. This piece not succeeding in either impact test is a major problem and in conclusion shows that the first case should have been used as the model chosen by the team to move forward in design.

5. References

1. Comparison of typical 3D printing materials. (2015). Retrieved April 27, 2019, from http://2015.igem.org/wiki/images/2/24/CamJIC-Specs-Strength.pdf
2. Overview of materials for High Density Polyethylene (HDPE). (n.d.). Retrieved April 27, 2019, from http://www.matweb.com/search/datasheet_print.aspx?matguid=f9470672aa5549cb9c7b157677d02062
3. Behalek, L., Lenfield, P., Seidl, M., Bobek, J., & Ausperger, A. (2012, October). FRICTION PROPERTIES OF COMPOSITES WITH NATURAL FIBRES, SYNTHETIC AND BIODEGRADABLE POLYMER MATRIX. Retrieved April 27, 2019, from http://nanocon2013.tanger.cz/files/proceedings/04/reports/722.pdf